Interpretative SOL modeling throughout multiple ELM cycles in DIII-D

A. O. Nelson[a,b,*], Z. A. Xing[a], O. Izacard[a], F. M. Laggner[b], E. Kolemen[a,*]

[a] *Princeton University, Princeton, NJ 08544, USA*
[b] *Princeton Plasma Physics Laboratory, Princeton, NJ 08543, USA*

Abstract

Coupling between the UEDGE (edge fluid model), GINGRED (grid generation) and CAKE (equilibrium reconstruction) codes opens the door for automated interpretative scrape-off-layer (SOL) analysis over entire discharges, providing information that is essential in efforts to couple the SOL to core transport codes. In this work, we utilize new developments in the autoUEDGE code [Izacard, O. *et al., 60th Annual Meeting of the APS Division of Plasma Physics* **53**, 11 (2018)] to investigate the behavior of the DIII-D SOL during the temporal evolution of an edge-localized mode (ELM) cycle. Modeled temperature and density profiles in UEDGE are automatically matched to experimental measurements by iteratively and self-consistently adjusting transport coefficient profiles in the plasma edge. This analysis is completed over multiple ELM cycles of a well-diagnosed discharge with long ($\sim$ 100 ms) inter-ELM periods. Directly after the ELM crash, a short period of high-density, low-temperature conditions is observed in Langmuir probe measurements at the outer divertor. This regime is associated with enhanced D_α emission and incident particle flux, suggesting that the divertor enters a period of high recycling after an ELM crash. After about $\sim$ 25 ms, divertor conditions return to their pre-ELM conditions and remain there for several tens of milliseconds. Using the autoUEDGE code, the SOL is modeled as a function of ELM cycle using upstream profiles as input. The 2D modeling successfully reproduces both divertor Thomson scattering measurements and the experimentally observed divertor dynamics. Though the recycling is kept fixed throughout the modeling, changes in particle fluxes are consistent with local experimental recycling changes induced by ELMs. Agreement between modeling and observation suggests a strong link between upstream profiles and the high-recycling divertor conditions directly following large type-I ELMs.

Keywords: UEDGE, SOL, ELMs, integrated modeling

1. Introduction

Tokamak plasmas can be broadly separated into two distinct regions: the confined plasma region, which is characterized by high densities and temperatures along closed field lines, and the scrape-off-layer (SOL), which exists along open field lines between the separatrix and the machine walls. The interplay between these two regions, which in H-mode is governed by an edge transport barrier, is important for obtaining high plasma performance while transporting exhaust and protecting machine walls. Notably, fueling from gas puffing and recycling at the walls must traverse the SOL in order to reach the hot core plasmas. Meanwhile, heat and particles flow outwards from the core plasma into the SOL, where they interact with colder neutral populations on their way to the divertor. Crucially, the dynamics of these relationships help set pressure gradients that prop up core performance while keeping acceptable heat fluxes to plasma-facing components. In this paper, we introduce first physics results from a novel 2D approach to investigate these dynamics.

In H-mode, a transport barrier forms near the boundary of these two regions, allowing steep gradients in the density and temperature profile to develop at the edge of the confined plasma region. While the H-mode pedestal improves plasma performance, it is limited by intense instabilities, called edge localised modes (ELMs), that temporarily relax the pedestal gradients by expelling plasma energy out of the confined region. Previous studies have identified the existence of a high-recycling regime directly after ELM crashes, linking SOL fueling to ELM events. At ASDEX Upgrade (AUG), differences in recycling and detachment were observed pre- and post-ELM and between the inner and outer strike points of an H-mode plasma [1, 2]. Similar observations at JET point out that ELMs induce both desorption and implantation of deuterium, leading to complicated inter-ELM fueling behavior [3]. On DIII-D, a dense, cold divertor plasma was produced after ELMs in UEDGE-MB modeling of the ELM cycle, which incorporates a Macro-Blob approach for filamentary non-diffusive transport [4].

Notably, recent 1D "closed box" simulations have used a coupling between the edge plasma code UEDGE and the wall reaction-diffusion code FACE to investigate the effect of an ELM-like heat pulse on divertor plasmas [5]. These simulations showed that outgassing from the machine walls during ELMs can be significant enough to impact the state

*Corresponding authors: anelson@pppl.gov, ekolemen@pppl.gov

of plasma detachment and that plasma neutrals play a large role in the heat transport in this state [5]. Of course, plasma detachment in turn also effects the core plasma, completing a connection between wall outgassing during ELM events and core plasma performance.

Not only do ELMs influence SOL plasma conditions, but SOL conditions can also impact ELM behavior on a recycling timescale [6]. In experiments at both JET and DIII-D, the development of a divertor sheath was found to limit energy loss from the pedestal during an ELM [7, 8]. Sheaths can also limit the heat flux to the wall, possibly even leading to the onset of detachment [9, 10]. Further, radiation in the divertor region, while necessary for protecting machine walls from strong heat fluxes, must be carefully controlled to avoid degradation of the density pedestal or plasma confinement [11, 12]. In short, numerous links have been established between SOL and core plasmas, all of which will need to be addressed in a burning plasma reactor.

To better understand the relationship between the SOL and the core region, a dynamic 2D edge physics model must be employed. However, reaching convergence in edge models is often difficult due to challenging geometries, uncertain neutral densities and sparse diagnostic measurements, among other challenges. In this work, we use a new algorithm [13], which automatically matches outer midplane (OMP) profiles of electron density and temperature by solving the UEDGE code [14], to investigate relationships between the pedestal and SOL as a function of ELM cycle. These novel algorithms represent a new capability to automatically run interpretive UEDGE simulations for a large number of time slices, opening the door for both dynamic and database SOL analysis in fusion reactors.

To demonstrate the potential capabilities of this code, we apply automated 2D UEDGE analysis to a controlled DIII-D discharge. In section 2 we present new experimental evidence for a high-recycling regime after type-I ELMs in DIII-D. When compared to previous work ([6, 7]), the high-recycling regime is found to last significantly longer ($\sim$ 25 ms), pointing to an additional effect beyond wall outgassing. An investigation of this effect is completed with the new autoUEDGE code [13], which is briefly explained in section 3. Results from the 2D modeling are presented in section 4, showing good agreement with experimental observations. Notably, since the observed divertor behavior is reproduced using only upstream profiles, a link between the inter-ELM divertor evolution and the upstream pedestal profiles can be established. Finally, conclusions and future work are discussed in section 5.

2. Experimental Methodology and Observations

The discharge discussed in this paper (DIII-D #174823) is a lower single-null H-mode with good diagnostic coverage and consistent ELMing behavior. In addition to the high-resolution Thomson scattering (TS) [15, 16] and charge-exchange recombination (CER) [17] data necessary

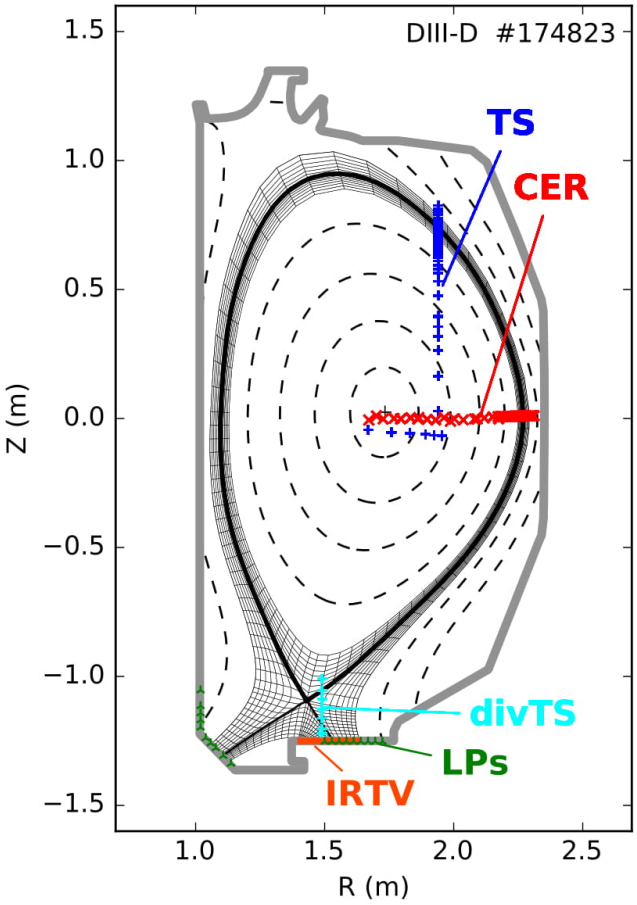

Figure 1: An overview of the considered diagnostics is overlayed on top of an example equilibrium and UEDGE grid. TS (blue) and CER (red) are used to construct core profiles, whereas divertor TS (cyan), ITRV (orange) and Langmuir Probes (green) are used for divertor analysis. D_α filterscopes aimed at the top and bottom divertor areas are not shown. (For interpretation of the references to color in this and future figure legends, the reader is referred to the web version of this article.)

for the reconstruction of accurate core profiles, divertor information was collected through divertor TS [18], Langmuir probes (LPs) [19], D_α filterscopes [20] and an infrared television (IRTV) camera [21]. Figure 1 shows the magnetic geometry for this discharge, as well as the locations of key core (TS and CER) and divertor (divertor TS, LPs and IRTV) diagnostics. An open, un-pumped divertor configuration was selected in order to provide improved access to divertor diagnostics. Further, no external gas puff is employed during the flattop of this discharge, so all particle sourcing comes from neutral beam injection (NBI) and recycling/outgassing at the walls.

As seen in the D_α trace presented in figure 2, the ELMs in this discharge are large, consistent type-I ELMs with a slow repetition frequency ($f_{\mathrm{ELM}} \sim 10$ Hz). In particular, the low ELM frequency allows the study of long-time scale evolution in the SOL with UEDGE, as is discussed below. Modulated NBI accounts for ~ 2.35 MW of injected power

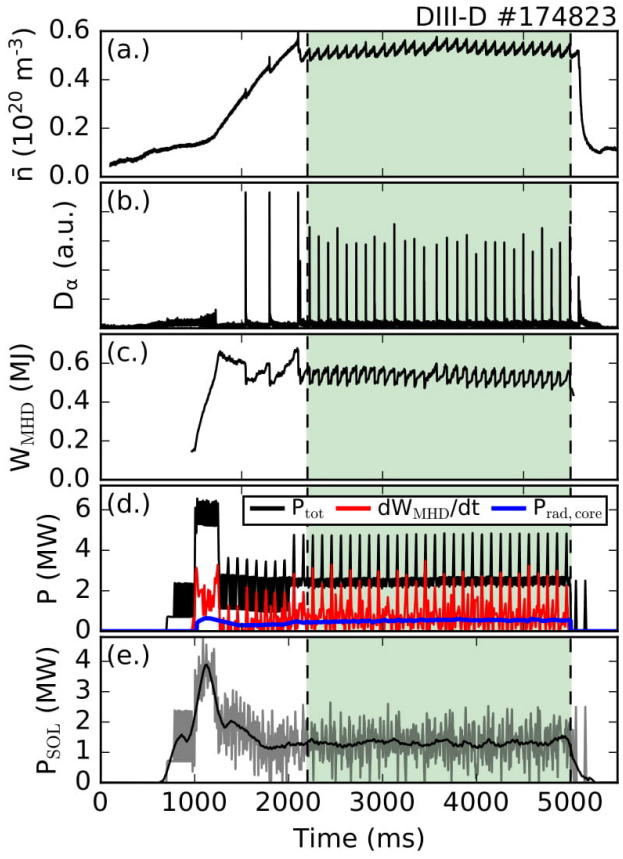

Figure 2: Time traces for a low ELM frequency (~ 10 Hz) plasma discharge are shown. The line-averaged density (a), shows strong correlation with slow consistent ELMing behavior observable in the D_α signal (b). The stored plasma energy (W_{MHD}) is shown in (c). The power radiated in the core $P_{\mathrm{rad,core}}$ and dW_{MHD}/dt are subtracted from the total injected power (d) to yield P_{SOL} - the power exiting the SOL (e).

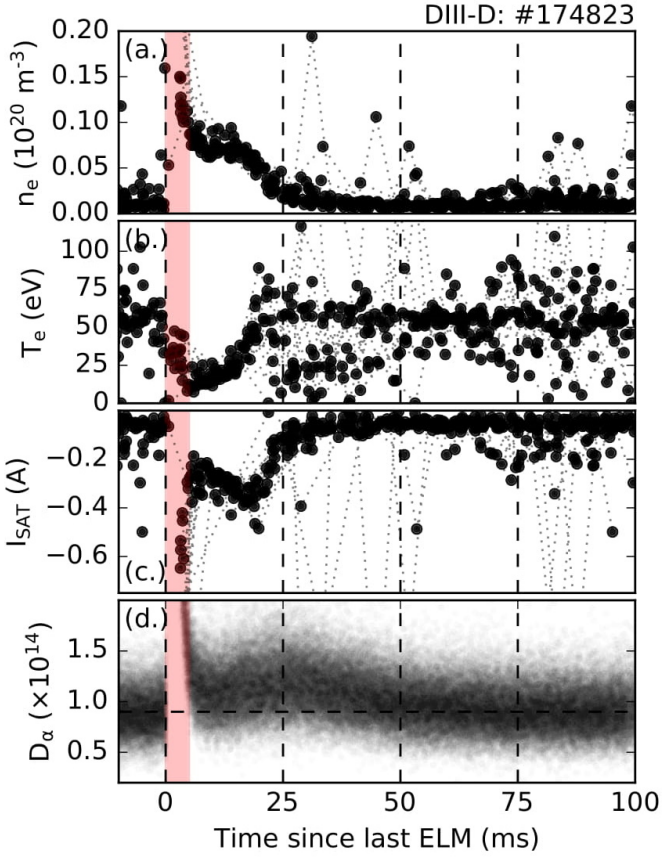

Figure 3: Plasma behavior in the outer divertor as a function of ELM-period. Density (a), temperature (b) and saturation current (c) are all read from a Langmuir probe near the outer strikepoint. The D_α measurement in (d) is taken from a filterscope aimed at the strikepoint location. The ELM crash is shaded in red.

during the flattop period of this discharge. An additional ~ 0.35 MW of Ohmic power yields a total input power of $P_{\mathrm{tot}} \sim 2.7$ MW. $P_{\mathrm{rad,core}}$ - the power radiated inside of the separatrix - is calculated at each time step by automatic fitting to the bolometer chords. The total MHD energy in the plasma (W_{MHD}) was calculated every 0.5 ms using unintegrated magnetic probe signals to avoid noise introduced by hardware integrators. The ELM-filtered time rate of change in W_{MHD} shown in figure 2-d is found to spike with blips in the beam modulation, which occur at regular intervals slightly faster than the natural ELM repetition rate. As a result, the total power entering the SOL given by

$$P_{\mathrm{SOL}} \equiv P_{\mathrm{tot}} - \frac{dW_{\mathrm{MHD}}}{dt} - P_{\mathrm{rad,core}} \quad (1)$$

is found to be nearly constant at $P_{\mathrm{SOL}} \sim 1.3$ MW throughout the analyzed period of the discharge, as shown in figure 2-e.

2.1. Inter-ELM divertor behavior

Repeatable inter-ELM divertor behavior on DIII-D is explicitly reported as a function of ELM-phase in figure 3. Data from a LP and D_α filterscope just beyond the outer strikeline is presented as a function of time elapsed since the last ELM. Before the ELM event, the outer strikeline is attached with low divertor electron densities ($n_{\mathrm{e}} \sim 1 \times 10^{18}$ m^{-3}) and high electron temperatures ($T_{\mathrm{e}} \sim 50$ eV) at the plate. However, directly after the ELM event (shown in red), the outer divertor goes through a temporary phase of high n_{e} ($\sim 1 \times 10^{19}$ m^{-3}), low T_e (~ 15 eV), and larger saturation current I_{SAT} reported by the strikeline LP. This immediate post-ELM phase lasts for ~ 25 ms and is accompanied by slightly enhanced D_α radiation, as seen in figure 3-d which shows a zoom-in of the D_α baseline as measured by a filterscope aimed at the outer strikeline position. At about ~ 25 ms after the start of the ELM event, LP measurements report a return to pre-ELM conditions which last until the start of the next ELM. D_α measurements recover the pre-ELM baseline at a slightly slower rate, returning to their pre-ELM state between ~ 25 and 50 ms after the ELM event. Throughout this discharge,

temperatures at the inner divertor remained low and almost unchanged throughout the ELM cycle. Inner divertor densities are slightly diminished after an ELM crash due to better attachment of the plasma, and again recover to their stationary values after ~ 25 ms.

Previous studies on DIII-D have reported increased divertor density after an ELM due to local generation of plasma at the divertor front [6, 7]. This behavior is similar to studies conducted on JET [3] and AUG [1, 2], where ELM crashes trigger a switch from a low-recycling to a high-recycling regime at the outer divertor. Further, recent 1D UEDGE calculations have shown significant outgassing from walls during ELMs [5]. In the case presented here, the enhanced D_α measurement reported immediately after an ELM event is a signature of increased recycling of ions originating from the ELM. During this time period, the saturation current on the outer divertor LPs is elevated, indicating an increased flux of particles to the divertor target. Simultaneously, high density and low temperature conditions suggest an increased cold plasma presence in front of the plate, which would result from increased recycling directly after the ELM event. However, this regime lasts longer than the typical neutral recycling timescale on DIII-D (defined as the timescale over which perturbations relax due to neutral loss at the target - a few ms on DIII-D [6]), suggesting that further effects from the upstream profiles may come into play as well.

2.2. Inter-ELM profile behavior

Inter-ELM behavior of the H-mode pedestal structure has been well documented on several machines [22–24]. Typically, the maximum n_e gradient recovers before the maximum T_e gradient, which occurs several milliseconds after the ELM onset. After gradient clamping, the height of the H-mode pedestal continues to grow until it reaches a hard limit set by peeling-ballooning instability constraints [25]. As such, two distinct phases of pedestal profile evolution exist: a quick recovery of the pedestal gradient that occurs directly after the ELM event and a slower growth of the density pedestal height that continues throughout the ELM cycle until global stability limits are reached.

For the discharge considered here, these two phases of pedestal growth can be observed in figure 4, where raw TS measurements of n_e and T_e are plotted as a function of the time elapsed since a preceding ELM. Both the n_e and T_e are plotted for individual TS channels at three locations inside the separatrix: the pedestal foot (black - bottom), the steepest gradient region (red - middle) and beyond the top of the pedestal (blue - top). At each location, a unique trend can be observed. During the ELM crash, n_e near the separatrix ($\psi_n = 0.99$) temporarily spikes before recovering its pre-ELM (stationary) value after ~ 5 ms. On similar timescales, the n_e gradient is flattened and recovered in the middle of the pedestal ($\psi_n = 0.96$). However, after an initial drop of $\sim 30\%$ at the ELM event, n_e inside of the pedestal top ($\psi_n = 0.89$) slowly recovers over a much longer timescale of ~ 100 ms, equivalent to the full ELM

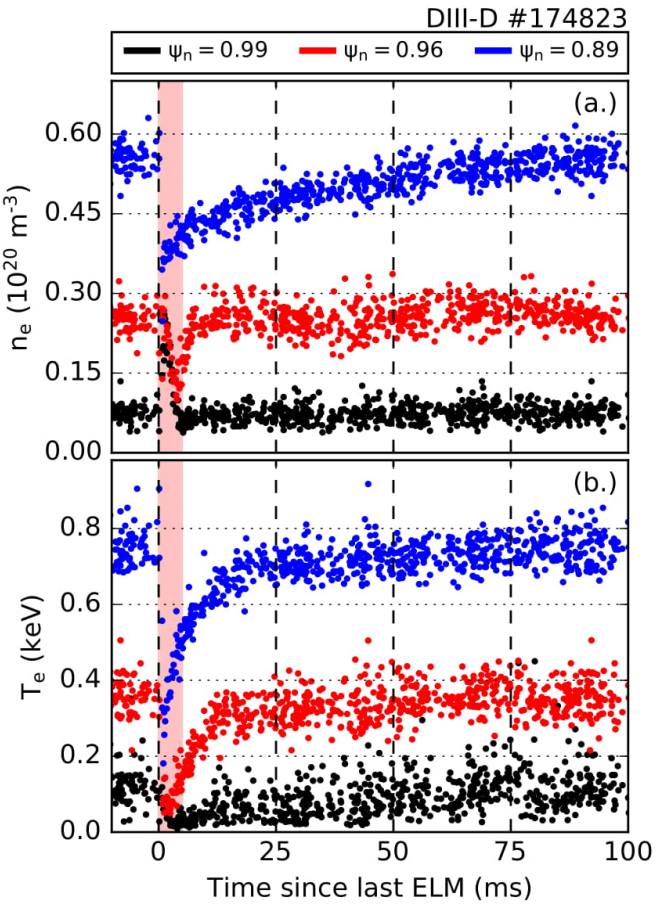

Figure 4: Electron density (a) and temperature (b) measurements as a function of time since the last ELM. Little change is observed at the separatrix (black), data in the middle of the pedestal (red) experiences a rapid rise after the ELM and data at the top of the pedestal (blue) rises on a slower timescale until the onset of the next ELM.

cycle. While the initial recovery of the T_e gradient after an ELM occurs over a longer time period (~ 15 ms) than the density gradient recovery, the T_e pedestal height saturates much quicker than the density pedestal, with only minor temperature gain after ~ 25 ms.

The timescales present in the inter-ELM core profile behavior create continuously changing profiles over the course of the ELM cycle. However, as none of these trends correlate directly with the abrupt change in divertor conditions observed at ~ 25 ms in figure 3, more investigation is required. The rest of this paper will be devoted to the study of SOL conditions with the UEDGE code using the experimental profiles from figure 4 as input. By automatically adjusting transport conditions to match changing experimental profiles, a link between pedestal and divertor evolution can be established.

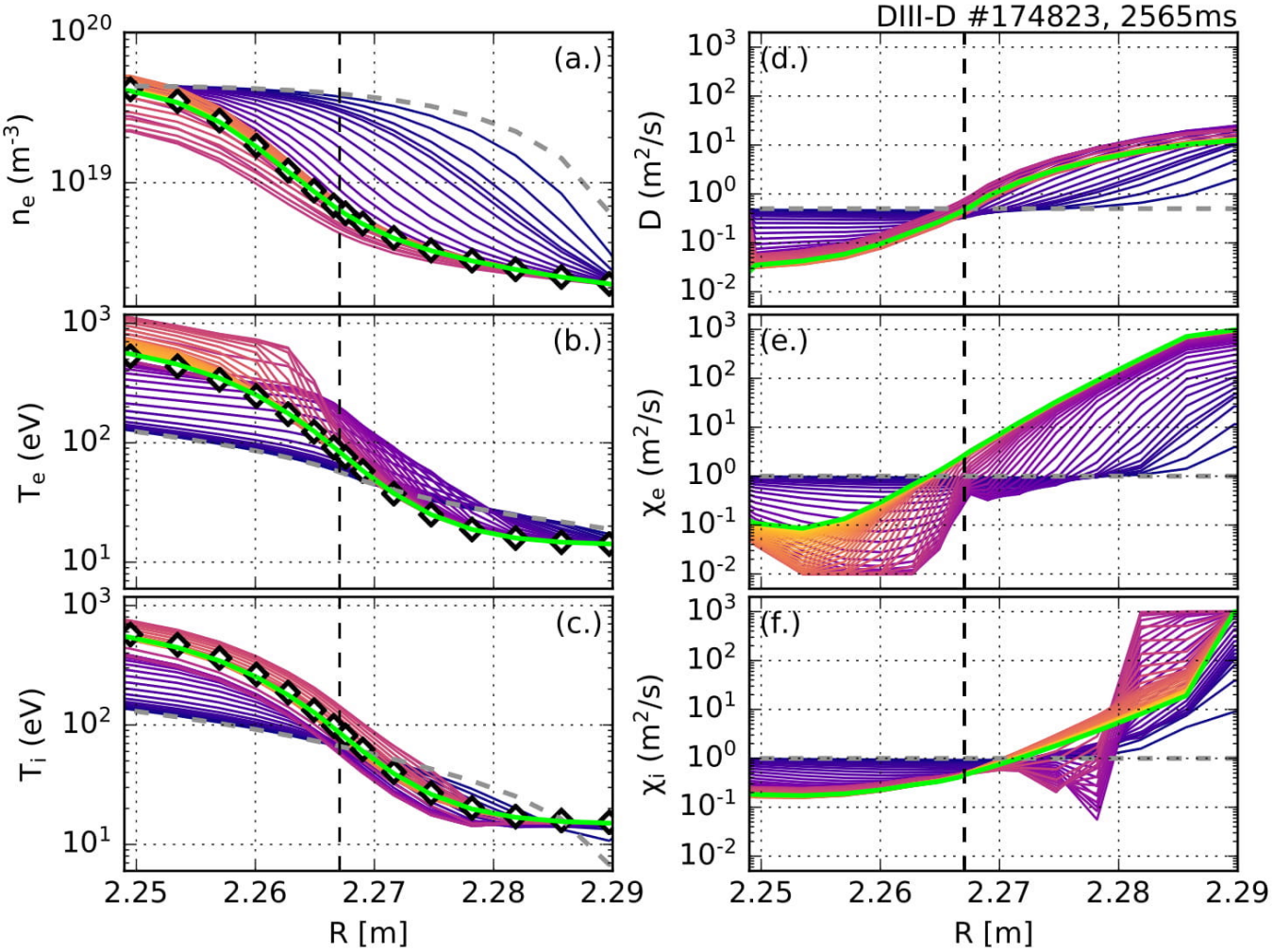

Figure 5: Modeled outer mid-plane (a) n_e, (b) T_e and (c) T_i profiles are shown for a single time slice taken midway through the ELM cycle. Initial guesses are given as a grey dashed line, which then evolve via the autoUEDGE algorithm (blue through yellow) towards the final profile (green) based on comparison with data (white diamonds). Due to diagnostic constraints, the experimental OMP T_i profile is defined by assuming a constant T_i/T_e ratio in the edge region. Also shown is the evolution of the corresponding anomalous transport coefficients: (d) D, (e) χ_e and (f) χ_i.

3. Code Description

In this work, we use a series of automated codes to run interpretative UEDGE as a function of time for several seconds during the flattop period of a DIII-D discharge (see green area in in figure 2). The automated procedure consists of three steps:

1. Kinetic equilibria are generated for each time step using the CAKE code [26], which has recently been developed and published at DIII-D.
2. A grid is generated for each equilibria using the GINGRED grid generator [27], which is available for public use through the OMFIT framework [28] and creates standardized grids for arbitrary 2D magnetic equilibria and plate geometries.
3. Finally, the autoUEDGE algorithm [13] is used to interpretatively solve UEDGE, a 2D fluid transport code [14], at each time step.

After completion, this algorithm provides a full 2D UEDGE solution for each time step included for analysis, opening the door for the dynamic study of 2D SOL evolution.

The equilibria used in this study are generated with the CAKE code, which was developed at DIII-D to automatically generate consistent and robust kinetic equilibria [26]. It is used instead of a manual kinetic equilibrium reconstruction workflow in order to eliminate user-induced variations between time slices. These equilibria are inspected for proper identification of the separatrix location, bootstrap current and pressure profiles. In future work, CAKE will be used to generate consistent kinetic equilibria for a large database of DIII-D discharges [26].

UEDGE is an implicit code that can converge and return multi-species 2D plasma equilibrium solutions from user-specified anomalous diffusion and convection trans-

port coefficient profiles [14, 29]. In the autoUEDGE model, we use a robust procedure to automatically converge the implicit UEDGE code to a solution within a few hours, as well as an additional loop that iteratively adjusts transport coefficient profiles to match the modeled density and temperature gradients to the experimentally measured values [13]. In each loop, radial profiles of the anomalous transport coefficients D (diffusion), χ_e (electron heat conductivity) and χ_i (ion heat conductivity), as well as the gas puffing rate, are adjusted towards convergence. This process is shown in figure 5, where the UEDGE-converged OMP profiles are shown for the three matched inputs (n_e, T_e and T_i). For each case, a standard starting guess for the anomalous transport coefficient (D, χ_e and χ_i, respectively) yields an initial solution, depicted with a grey dashed line. Note that transport profiles used in this work are only 1D - poloidal variation of transport coefficients will be included in future work. The transport profiles are then iteratively adjusted based on comparisons between the gradients of the UEDGE solution (blue to yellow lines) and the experimental input (white diamonds) until a final profile-matching solution (green line) is achieved. The anomalous transport coefficients used in this process, which are bounded between 10^{-2} and $10^{3}\,\mathrm{m}^2/\mathrm{s}$, are also included in figure 5, showing evolution towards a final interpretive profile. During this process, it is important to note that a numerical gas source is also varied in order to achieve neutral densities within a pre-specified target range, as is discussed in more detail below. In comparison to the literature [30], this algorithm includes damping on top of the iterative modifications and uses gradient matching instead of flux or profile matching in order to enhance core matching in priority before SOL matching and to improve iterative optimization. Further, we impose hard limitations to avoid unphysically large transport coefficients values $> 1000\,\mathrm{m/s}^2$, as seen in figure 5-f. In all cases used here, the normalized root-mean-square deviation between the final solution and the experimental profiles is $< 5\%$ after ~ 50 iterations.

Several assumptions are made during this process to facilitate better convergence rates. For the work presented here, flux (Neumann) boundary conditions were imposed on both the power and particle flow from the core, as set by typical experimental values at the grid edge ($\psi_n = 0.94$). These were held constant as a function of time, as suggested by the steady P_{SOL} and constant density gradient traces reported in figure 2. At the outer SOL boundary, temperature and density (Dirichlet) boundary conditions are used according to TS measurements at that location. The impurity content is held constant at 2% carbon, consistent with standard DIII-D operation. For the ELM-cycle investigations, the plate recycling is held constant over time at 0.99, and no additional surface effects such as sputtering or chemical erosion are considered. Though there was no experimental gas puffing in this discharge, a numerical gas puffing parameter, which includes additional recycling, wall outgassing and neutral flux from the far SOL, was allowed to vary self-consistently in time, as discussed below. Input electron profiles are produced using the OMFITprofiles [31] framework, where core and SOL TS data was fit to the standard `mtanh` shape [32]. Ion temperatures were not available in the SOL, so a constant T_i/T_e ratio (defined from measurement at the pedestal top, $T_i/T_e \sim 1-1.3$) was assumed throughout the pedestal and SOL. Drifts are not included in the results presented here but will be incorporated into future work. The grid domain encompasses the full plasma cross section between $\psi_n = 0.94$ and $\psi_n = 1.07$, as shown in figure 1.

Each simulation was run with a fixed divertor recycling coefficient to avoid biasing the 2D model and the particle flux at the UEDGE core boundary is determined by experimental particle balance and held constant for each time slice. However, as ionization rates and densities iteratively change due to evolution in D, χ_e and χ_i, an additional free parameter is needed to maintain experimentally acceptable particle balance across the full UEDGE grid. As such, the gas input to the SOL is adjusted in each iteration to match the simulation to a user-specified neutral density range. This gas input value is not equivalent to the gas puff measured at the machine valves (which was zero throughout this discharge,) but rather allows for neutral flux from the far SOL as well as additional plate recycling and wall outgassing not already capture in the fixed-recycling model. This value is self-consistently adjusted in the autoUEDGE algorithm according to two constraints: (1) to allow for particle balance with the fixed core boundary particle flux and (2) to adjust the neutral density at the separatrix to within a user-specified range. Iteration of this parameter alleviates potential particle flux imbalances caused by the misalignment between the outer grid of UEDGE and the machine wall and compensates for unknown physical boundaries that are fixed or scalar by assumptions (such as 1D profiles of all quantities on the wall.) On top of that, it is possible to add a physically interpreted gas puff to reproduce experimental local gas puffing at specific locations, though that is not done in this work due to the absence of gas puffing in the studied discharge. Excluding the plasma profiles, all other factors influencing the neutral density are held constant for each simulation, so the model gas puffing acts broadly at setting global particle balance.

In this work the UEDGE framework is used to implicitly evolve the plasma state in time towards a steady-state solution for each time slice, so there is a minimum timescale that can be obtained regarding the modeling of plasma dynamics with UEDGE. In the context of this work, this minimum timescale was determined by comparing the change in density between consecutive time slices to the calculated diffusion profile at each time step. If the change in density could not be explained by the modeled interpretive diffusion rates, the dynamics were assumed to be too fast to be accurately captured by the existing autoUEDGE model. With this under consideration, the autoUEDGE model was found to be adequate in describing

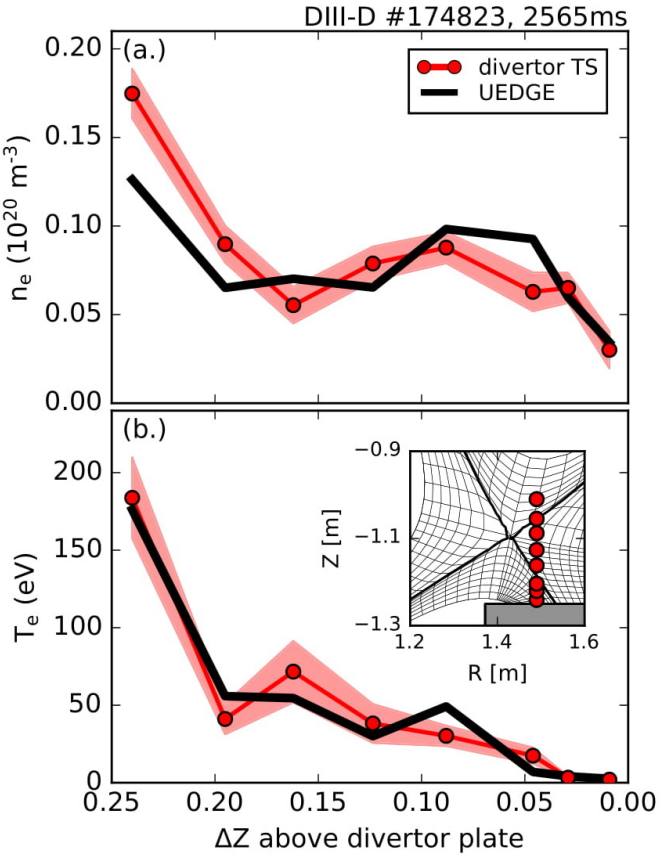

Figure 6: Divertor Thomson measurements (red) of electron density (a) and temperature (b) are compared to synthetic diagnostics from UEDGE (black) for a single time slice mid-way through the ELM cycle, showing good agreement between modeling and experiment.

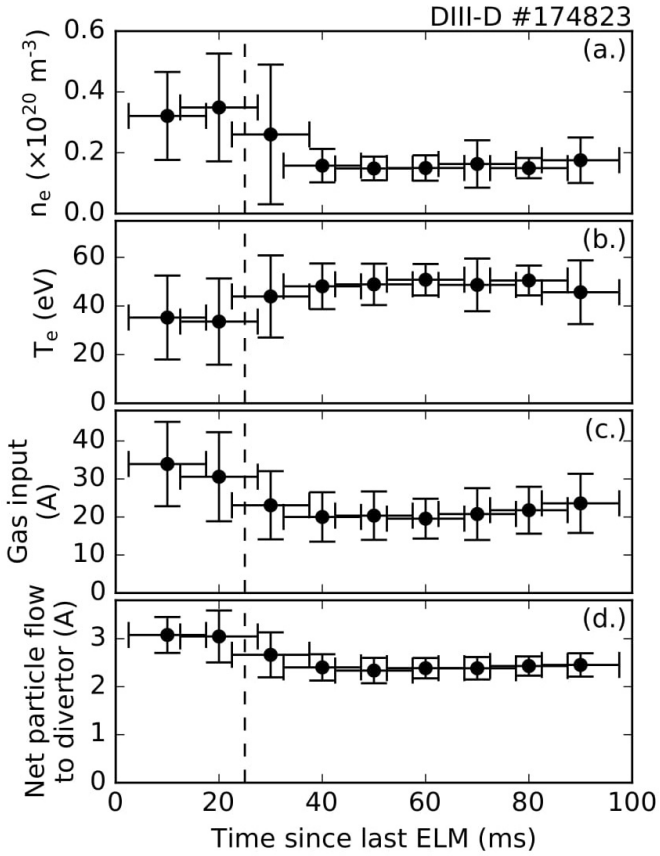

Figure 7: ELM-synced averages of divertor parameters from ~ 125 converged UEDGE simulations. (a) The peak n_e along the outer divertor shows the same behavior as the LP traces in figure 3, with elevated divertor densities before ~ 25 ms. Also shown are the (b) the divertor T_e, (c) the external gas source determined by the code and (d) the particle flow to the outer divertor. A dashed at 25 ms is included to guide the eye.

the inter-ELM dynamics for DIII-D discharge #174823 at all times except for directly after ($\lesssim 10$ ms) an ELM crash. These fast dynamics have been studied with UEDGE before [4, 5], but this is outside of the scope of the current work, which focuses on the slower inter-ELM evolution. As such, all dynamics < 10 ms after each ELM event (where the experimental profiles are changing the fastest) are ignored in this paper. In future work, results obtained in this manner will be compared with time-dependent UEDGE simulations. Potential transport effects from dynamically evolving magnetic equilibria may further complicate this analysis if the equilibrium is changing quickly, though this is not expected to play a large role in the analysis presented here.

4. Results and Discussion

Utilizing the above automated UEDGE procedure, the 2D transport model was solved every 5 ms during the ~ 3 s flattop period shown in green in figure 2. During this period, the plasma parameters are all held constant and the only perturbations introduced into the plasma are the slow (~ 10 Hz) ELMs. Since the background plasma is held constant, statistics regarding the slow inter-ELM evolution are gathered by averaging together results from time slices according to the time elapsed since the last ELM. As such, the results presented below are obtained from averages across multiple independent autoUEDGE time slices.

Before averaging, each time slice considered here is inspected individually for convergence. The relative error between the UEDGE results and the experimental inputs is calculated for each of the input OMP profiles (n_e, T_e and T_i) at each radial location shown in figure 5. If the relative error for any profile at any radial location is greater than 10%, the time slice is discarded in the final analysis. Further, all time slices within 10 ms of an ELM event are ignored. Approximately 30% of the initial time slices meet this requirement, yielding ~ 125 converged profiles across the full ELM cycle for further analysis.

Divertor measurements from LPs, IRTV and divertor TS were not included as input and were instead used as further comparison for the UEDGE solutions by means of a synthetic diagnostic. In figure 6, TS measurements

in the divertor are compared to a synthetic diagnostic on a converged autoUEDGE run for a single time slice approximately halfway through the ELM cycle. Both the magnitude and shape of the divertor TS profile are well-captured by the automated 2D model, showing increased density along the strikeline and agreement with wall and core boundary conditions. Note that the TS measurements in the private flux region (see inset of figure 6) report lower T_e near the divertor plate than the strikeline Langmuir probe measurements presented in figure 3. This 2D variation of the SOL T_e is well captured in the UEDGE model. Similar agreement was found comparing IRTV measurements and heat flux profiles from UEDGE, with the total integrated heat flux on the outer divertor matching experiment within $\sim 30\%$.

In order to determine the divertor behavior as a function of ELM cycle, results from ~ 125 converged UEDGE runs were averaged together according to the time elapsed since a previous ELM. Averages were computed with 15 ms windows every 10 ms after an ELM event. Traces of the averaged divertor parameters as a function of ELM cycle are shown in figure 7. The results showed qualitative similarity to the LP traces presented in figure 3 at the outer divertor, with modeled divertor densities spiking and temperatures dropping for ~ 25 ms after the ELM crash. In figure 7-a, the peak electron density along the outer divertor is plotted, showing a clear rise in the divertor density directly after an ELM crash. As in the LP data, this high-density regime lasts for ~ 25 ms (marked with a dotted line) before returning to stationary values. Correspondingly, the divertor T_e in both the LP data and the autoUEDGE model is diminished for approximately ~ 25 ms after an ELM. Unique to the modeled data, the increase in the divertor density was accompanied by a slight increase in the upstream separatrix density $n_{e,sep}$.

As discussed above, controls on the neutral particle density are limited to a single 0D parameter defined as the gas puffing rate. Since the modeled recycling and core particle flux are held constant for each simulation, variations in the gas puffing rate can be interpreted as a change in the edge particle flux boundary condition that is necessary to reproduce the input experimental profiles. For example, 1D UEDGE simulations have shown that, during ELM events, outgassing from the machine walls can be significant [5], and observations on DIII-D have reported changes in wall recycling during and immediately after ELMs [6, 33]. In our model, since recycling is held constant, any post-ELM changes in particle flux in the divertor that is required to satisfy particle balance must manifest as an increase in the gas puffing rate. The ELM-averaged gas input is plotted in figure 7-c as a function of ELM cycle for times > 10 ms after the previous ELM, showing an $\sim 150\%$ increase in the input particle requirement directly after the ELM crash. Note that the majority of this input gas enters from the UEDGE outer wall. However, the net particle flow to the outer divertor (ie. ion flux - neutral return) is also elevated up to ~ 25 ms after the ELM crash (see figure 7-d), indicating an increased divertor particle demand after the ELM event that lasts longer that the typical neutral recycling timescale on DIII-D. The increased particle demand in our model is consistent with an increase in the recycling flux at the outer divertor: increasing gas puff in autoUEDGE produces larger particle fluxes in the plasma and therefore higher sourcing, as indicated by the increased particle flow at the divertor wall. While the recycling coefficient itself is not allowed to vary in time in these simulations, an increase in the required input gas is consistent with an increase in the incoming particle flux from the outer divertor.

SOL power balance as a function of the ELM cycle was also briefly investigated. Averaged power flowing into the SOL from the core is approximately constant, though consistently $\sim 2\%$ higher in the middle of the ELM cycle. While power flows to the inner and outer divertor are constant as a function time, less power ($\sim 90\%$ of the pre-ELM value) flows to the main chamber wall directly after the ELM crash. This results in a slight increase in the power radiated in the SOL after an ELM crash, as is expected from the higher densities during that time period.

Taken together, these results lead to several conclusions. First, remarkable agreement between modeled and experimental divertor data can be achieved through the automatic matching of OMP profile gradients with the autoUEDGE code, as is shown in figure 6. This opens the door for a new variety of edge code studies that are based on a large number of converged UEDGE runs. Second, high divertor densities directly following a type-I ELM are reproduced in concert with larger divertor particle fluxes, suggesting that a ~ 25 ms high-recycling regime is established after the ELM. Finally, since the experimental inter-ELM divertor dynamics are reproduced providing only the upstream profiles as input, a concrete link between the evolution of the upstream and divertor profiles is established. In reality, a complex mix of effects from both increased recycling and upstream profile evolution will determine the exact inter-ELM SOL dynamics.

5. Conclusion

Divertor dynamics are presented as a function of the ELM cycle for a DIII-D discharge with large and slow (~ 10 Hz) ELMs. After an ELM crash, a period with high densities and low temperatures is observed in the outer divertor, consistent with the temporary establishment of a high-recycling regime. The post-ELM state lasts for ~ 25 ms (much longer than the timescale of recycling equilibration set by the neutral loss from the target region - a few ms on DIII-D [6]), suggesting that upstream profile recovery may be linked to the divertor dynamics. Density and temperature profiles are observed to reach gradient saturation on a faster timescale, though peak pedestal values continue to evolve throughout the inter-ELM period.

To inspect the link between the pedestal and divertor, the autoUEDGE code [13] is used to model the quasi-

stationary SOL as a function of ELM cycle, using only OMP profiles as input. Under fixed boundary conditions, autoUEDGE is able to reasonably predict changes in the divertor at times > 10 ms after a type-I ELM, suggesting that the input upstream profiles are indeed linked to inter-ELM divertor evolution. Further, the 2D modeling reproduces an increase in both the divertor density and the particle flux to the divertor plate directly after the ELM crash, consistent with the establishment of a high-recycling regime. Future work will involve additional development of the autoUEDGE algorithm to include drifts, recycling changes, and improved impurity models in order to better constrain and identify SOL behavior, opening the door for potential database studies with interpretive UEDGE modeling.

Acknowledgments

The authors would like to acknowledge helpful discussions with E.D. Emdee and X. Zhang at Princeton Plasma Physics Laboratory, A. Järvinen at Lawrence Livermore National Laboratory and A. Leonard at General Atomics. Part of data analysis is performed using the OMFIT integrated modeling framework [28, 31]. Data used in this study was collected with DIII-D diagnostics operated by General Atomics, Princeton Plasma Physics Laboratory, Lawrence Livermore National Laboratory, Sandia National Laboratories, Oak Ridge National Laboratory and the University of California San Diego. This material is based upon work supported by the U.S. Department of Energy, Office of Science, Office of Fusion Energy Sciences, using the DIII-D National Fusion Facility, a DOE Office of Science user facility, under Awards DE-AC02-09CH11466, DE-SC0015480, DE-SC0015878 and DE-FC02-04ER54698.

Disclaimer

References

1. Wischmeier, M. et al. *J. Nucl. Mater.* **363-365,** 448–452 (2007)
2. Laggner, F. M. et al. *Plasma Phys. Control. Fusion* **60,** 025002 (2018)
3. Brezinsek, S. et al. *Physica Scripta* **T167,** 014076 (2016)
4. Pigarov, A. Y. et al. *Phys. Plasmas* **21,** 062514 (2014)
5. Smirnov, R. D. et al. *Phys. Plasmas* **27,** 032503 (2020)
6. Fenstermacher, M. E. et al. *Plasma Phys. Control. Fusion* **45,** 1597–1626 (2003)
7. Leonard, A. W. et al. *Phys. Plasmas* **10,** 1765 (2003)
8. Loarte, A. et al. *Plasma Phys. Control. Fusion* **44,** 1815 (2002)
9. Campanell, M. D. et al. *Phys. Rev. Lett.* **122,** 015003 (2019)
10. Masline, R. et al. *Phys. Plasmas* **27,** 092505 (2020)
11. Kallenbach, A. et al. *Plasma Phys. Control. Fusion* **55,** 12041 (2013)
12. Beurskens, M. N. et al. *Nucl. Fusion* **56,** 056014 (2016)
13. Izacard, O. et al. *60th Annual Meeting of the APS Division of Plasma Physics* **53,** 11 (2018)
14. Rognlien, T. D. et al. *J. Nucl. Mater.* **196-198,** 347–351 (1992)
15. Ponce-Marquez, D. M. et al. *Rev. Sci. Instrum.* **81,** 10D525 (2010)
16. Eldon, D. et al. *Rev. Sci. Instrum.* **83,** 10E343 (2012)
17. Chrystal, C. et al. *Rev. Sci. Instrum.* **87,** 11E512 (2016)
18. Glass, F. et al. *Rev. Sci. Instrum.* **87,** 11E508 (2016)
19. Watkins, J. G. et al. *Rev. Sci. Instrum.* **79,** 10F125 (2008)
20. Colchin, R. J. et al. *Rev. Sci. Instrum.* **74,** 2068 (2003)
21. Hill, D. N. et al. *Rev. Sci. Instrum.* **59,** 1878–1880 (1988)
22. Burckhart, A. et al. *Plasma Phys. Control. Fusion* **52,** 105010 (2010)
23. Diallo, A. et al. *Phys. Plasmas* **22,** 056111 (2015)
24. Laggner, F. M. et al. *Nucl. Mater. Energy* **19,** 479–486 (2019)
25. Snyder, P. B. et al. *Phys. Plasmas* **16,** 056118 (2009)
26. Xing, Z. A. et al. *Fusion Eng. Des.,* in review
27. Izacard, O. et al. *arXiv* **1705.05717v2** (2017)
28. Meneghini, O. et al. *Nucl. Fusion* **55,** 083008 (2015)
29. Rognlien, T. D. et al. *Phys. Plasmas* **6,** 1851–1857 (1999)
30. Canik, J. M. et al. *J. Nucl. Mater.* **415,** S406–S412 (2011)
31. Logan, N. C. et al. *Fusion Sci. and Technol.* **74,** 125–134 (2018)
32. Groebner, R. J. et al. *Nucl. Fusion* **41,** 1789 (2001)
33. Bykov, I. et al. *Physica Scripta* **2020,** 014058 (2020)